



1

2 Supporting Information for

3 Hierarchical woven fibrillar structures in developing single gyroids in butterflies

4 Anna-Lee Jessop, Peta L. Clode, Martin Saunders, Myfanwy E. Evans, Stephen T. Hyde, James N. McPherson, Kasper S.
5 Pedersen, Jacob J.K. Kirkensgaard, Nipam H. Patel, Kyle A. DeMarr, William O. McMillan, Bodo D. Wilts, and Gerd E.
6 Schröder-Turk.

7 Corresponding Author name.

8 E-mail: annie.jessop@murdoch.edu.au

9 This PDF file includes:

- 10 Figs. S1 to S9
- 11 Tables S1 to S2
- 12 Legends for Movies S1 to S2
- 13 Legends for Dataset S1 to S3
- 14 SI References

15 Other supporting materials for this manuscript include the following:

- 16 Movies S1 to S2
- 17 Datasets S1 to S3

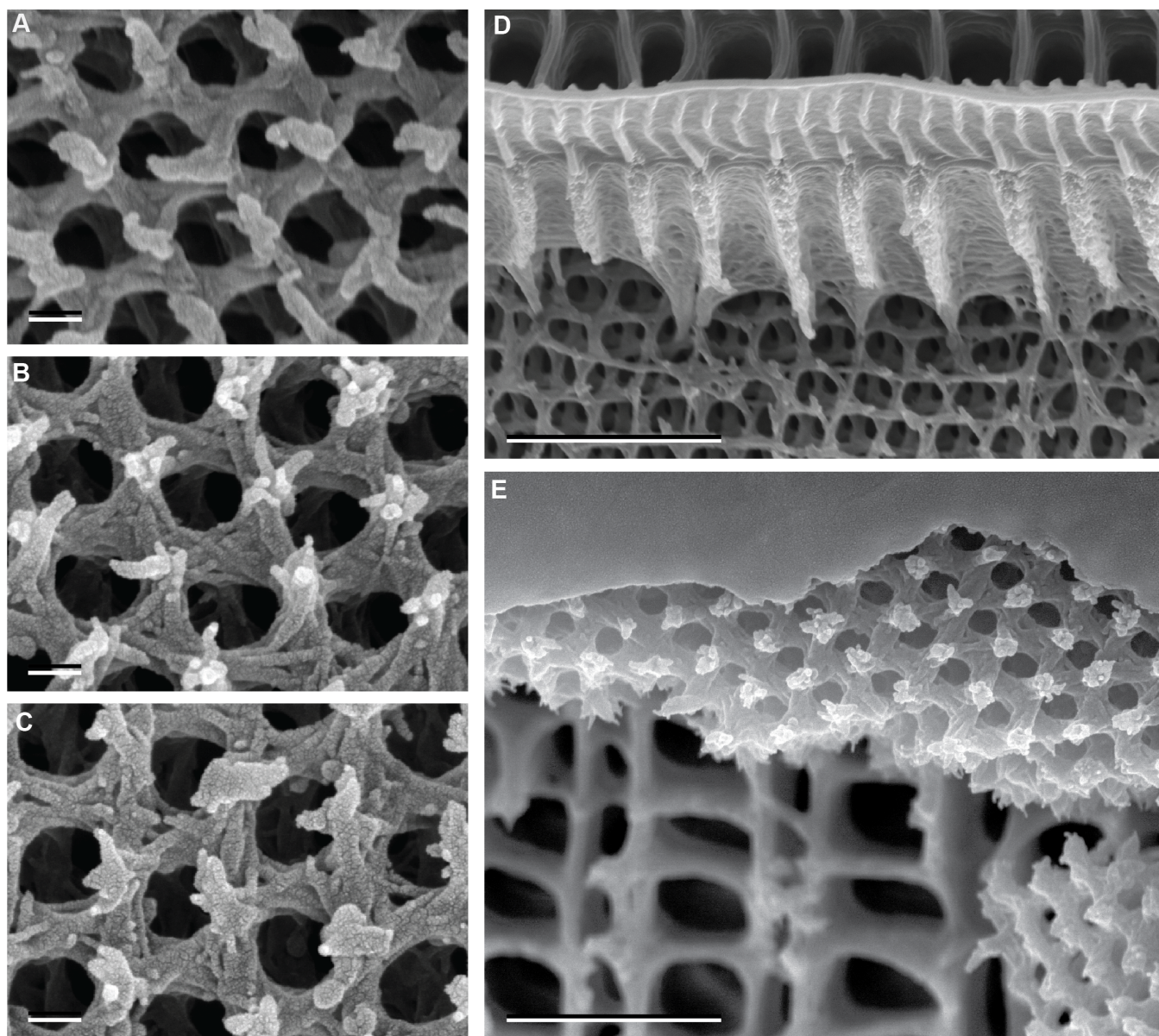


Fig. S1. SEM images of critical-point dried samples demonstrating the variation in fibre numbers. (A–C) SEM images of samples taken at day 12 (A), day 13 (B), and day 15 (C), showing a change in the number of entangled fibres throughout development. (D, E) The fibrous gyroid network adjacent to the upper lamina (D) is comprised of fewer fibres than the network adjacent to the lower lamina (E).

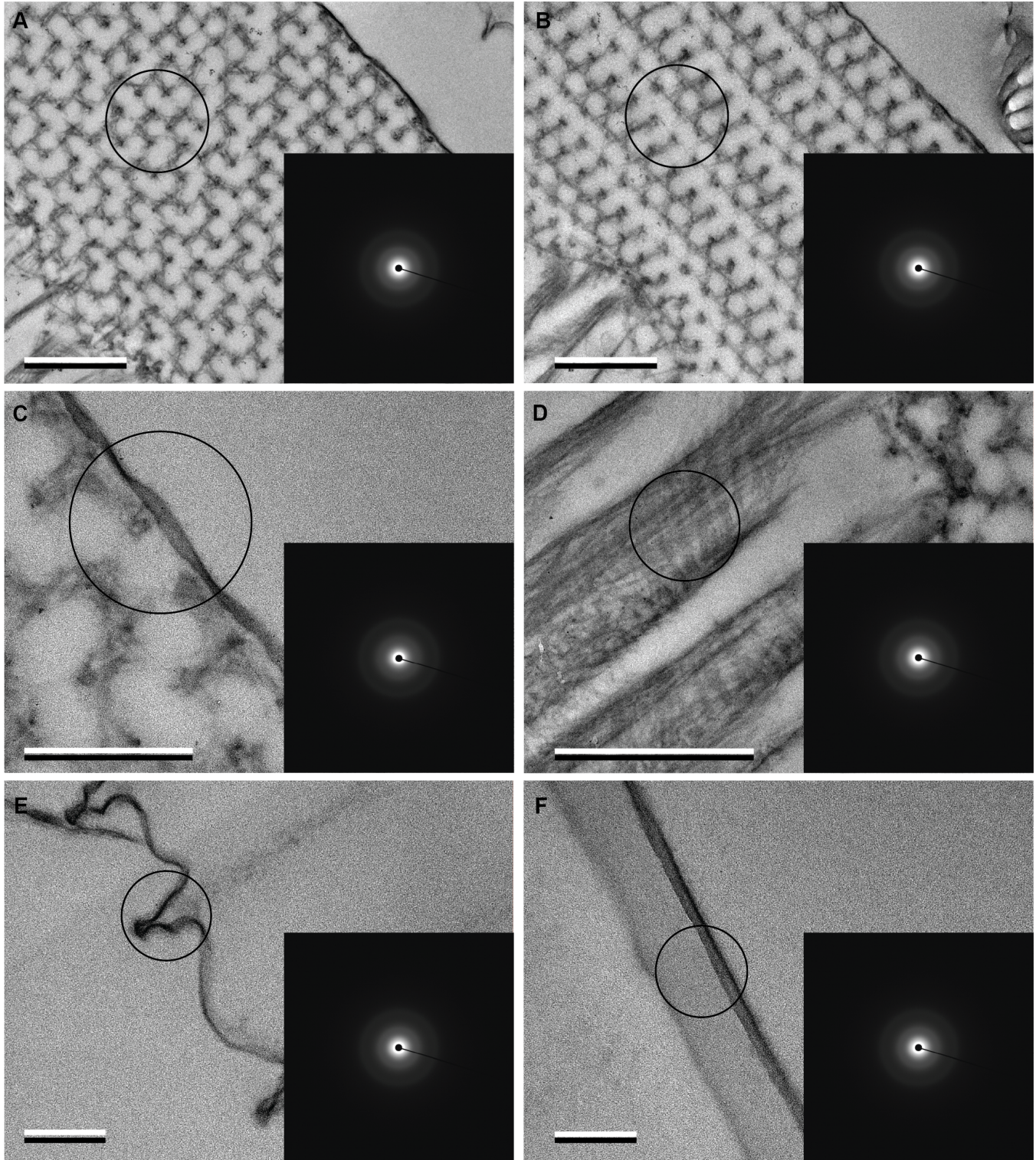


Fig. S2. TEM and SAED data of *Parides sesostris* samples fixed at day 15: (A,B) Green gyroid-containing scale cells with the diffraction mask set to regions that only contain gyroid fibres. (C,D) Green gyroid-containing scale cells with the diffraction mask set to include the lower lamina and the diffuser, respectively. (E,F) Black ground scale cells, with the mask focused on the upper ridges and the lower lamina. Analyses were carried out on resin embedded, 2% osmium tetroxide stained samples that were sectioned to a thickness of 250 nm. The black circle in the TEM images indicates the aperture (mask) used for the diffraction analysis. The insets show the scattering pattern obtained for each measurement (in order to exclude the possibility that the presence of osmium tetroxide in the samples may have obscured the signal, SAED was conducted also on samples prepared without osmium tetroxide; the resulting diffraction patterns showed no discernible difference to those prepared with osmium tetroxide.) Scale bars = 1 μm (A,B,D), 500 nm (C), and 200 nm (E,F).

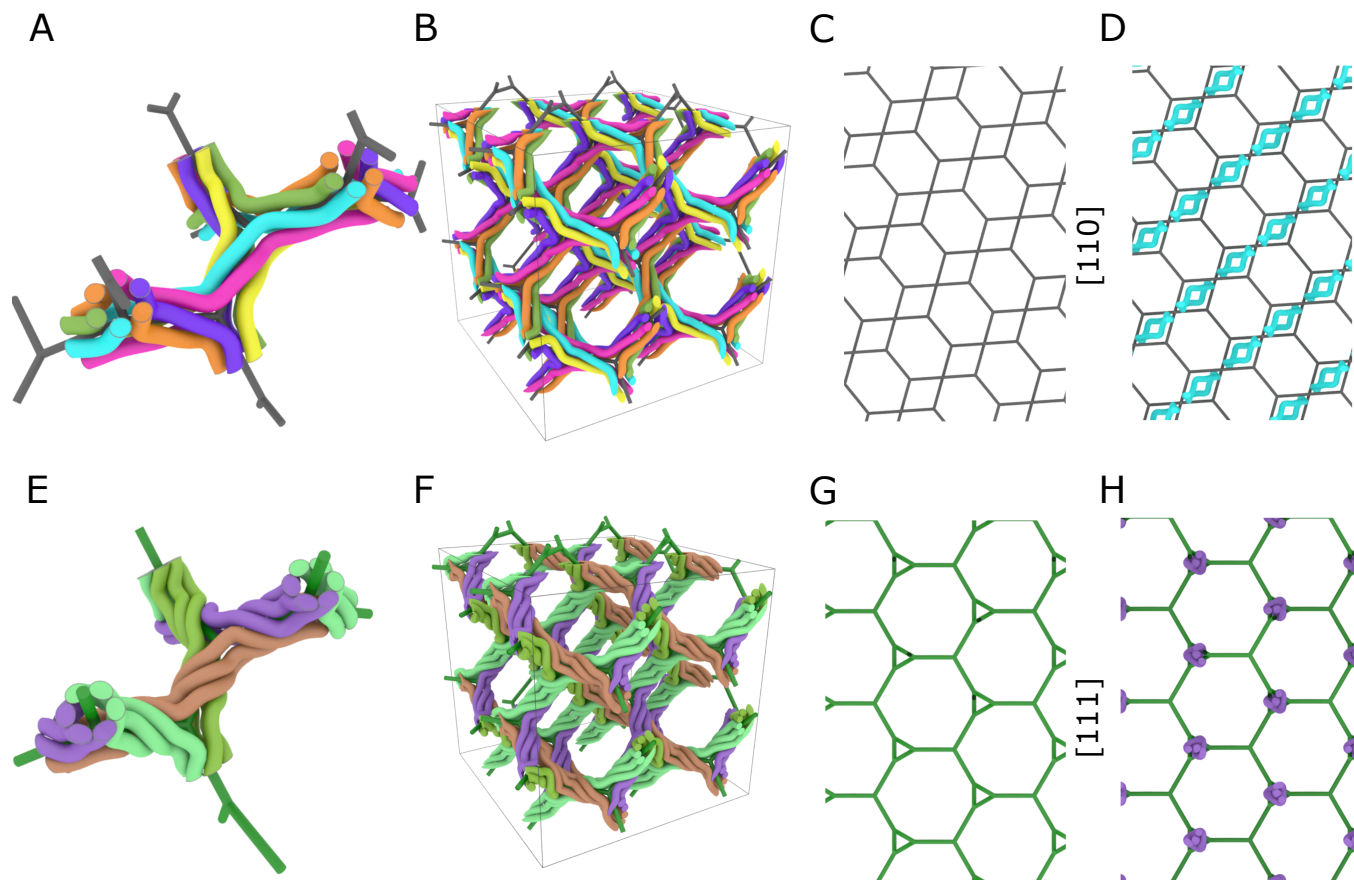


Fig. S3. Comparison of two geometric models $(\frac{0.8}{6})^6$ (A–D) and $(\frac{1.8}{6})^6$ (E–H) for 6-threaded weavings around the *srs* graph of the gyroid: (A,B) Small section and 2^3 translational unit cells of the $(\frac{0.8}{6})^6$ model; (C) the *srs* graph projected onto the [110] plane; (D) The $(\frac{0.8}{6})^6$ model breaks up into individual deformed helices along the six [110] directions; this image shows all those helices (in cream) that run along the [110] direction perpendicular to the paper. (E,F) Small section and 2^3 translational unit cells of the $(\frac{1.8}{6})^6$ model; (G) the *srs* graph projected onto the [111] plane; (H) The $(\frac{1.8}{6})^6$ model breaks up into individual triplets of deformed helices along the 4 [111] directions; this image shows all those helices (in purple) that run along the [111] direction perpendicular to the paper; each purple point corresponds to a bundle of three (triplet) helices revolving around the corresponding [111] axis.

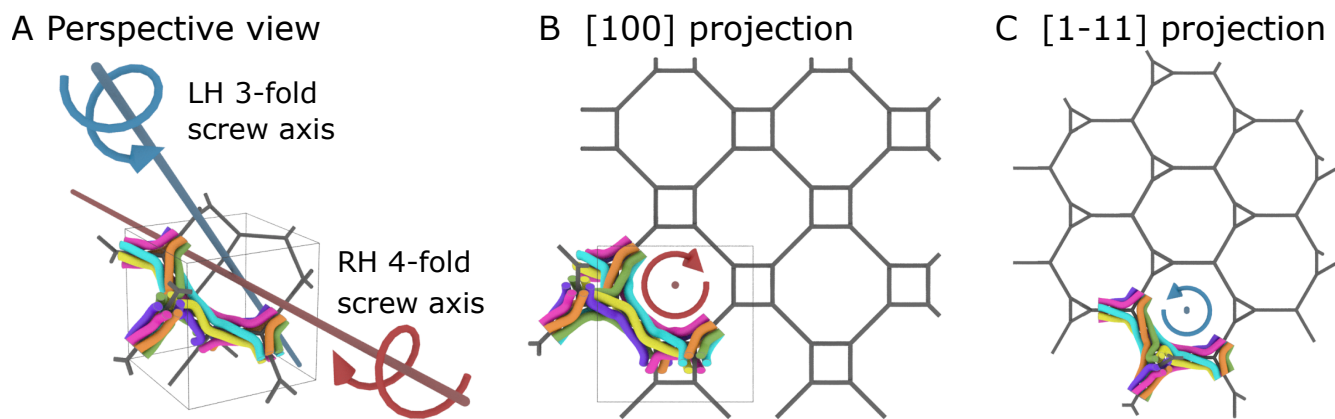


Fig. S4. Illustration of the enantiomeric type (chirality) of the models shown in supplementary figure S3 and in Figure 4 of the main manuscript. Throughout this work, we have used a 'right-handed' srs net, i.e. a network where the 4-fold and 3-fold screw axis shown in (B) and (C) are right-handed and left-handed, respectively. This is also the same enantiomer as is shown in (1) (Fig 2), with the same colour scheme as in that reference used here. Note the additional complication, described in detail in (1), that there are further 4-fold and 3-fold screw axes (centred in the squares in the [100] projection and in the triangles in the [111] projection, respectively); these are not marked here; these are not shown here. The section of the weaving shown here is the same as in supplementary figure S3(A). The screw rotational sense indicated by the curved arrows in (B) and (C) is for an axis pointing into the page. The projection in (C) is, strictly speaking, along the $(\bar{1}\bar{1}1)$ direction as indicated; however, this is equivalent to the (111) direction.

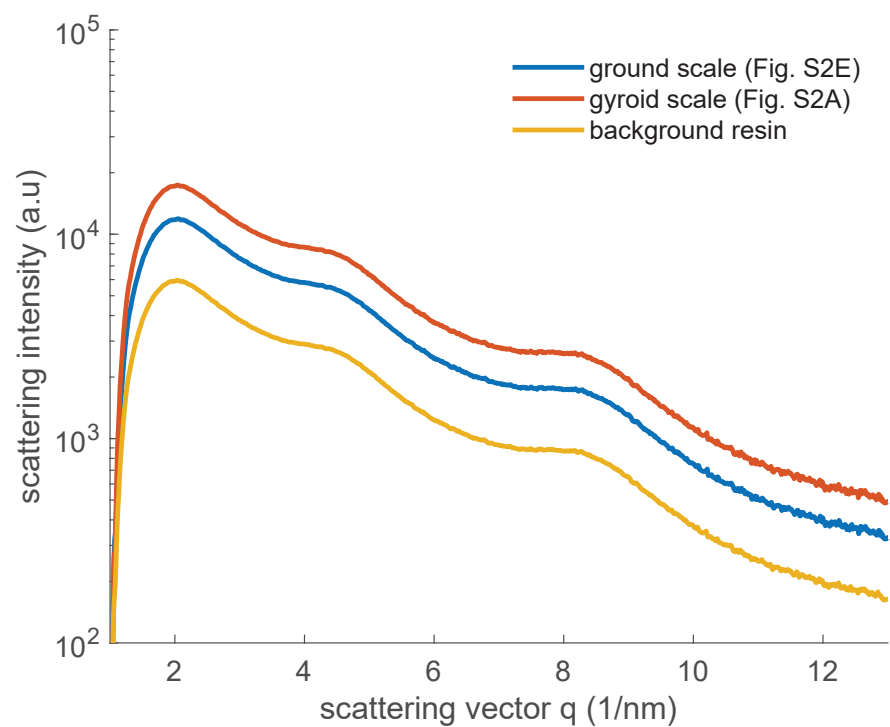


Fig. S5. Azimuthally averaged scattering intensities of the electron diffraction data of the measurements shown in Supplementary Figure S2, of fixed tissue of the developing butterfly at day 15. Measurements are shown for the data of a ground scale (Fig. S2E), of a gyroid forming scale (Fig. S2A) and of the background, that is, of a sample that only contains the resin used in these experiments. This presentation of the data provides further demonstration that the butterfly diffraction data contain no discernible features beyond the resin background.

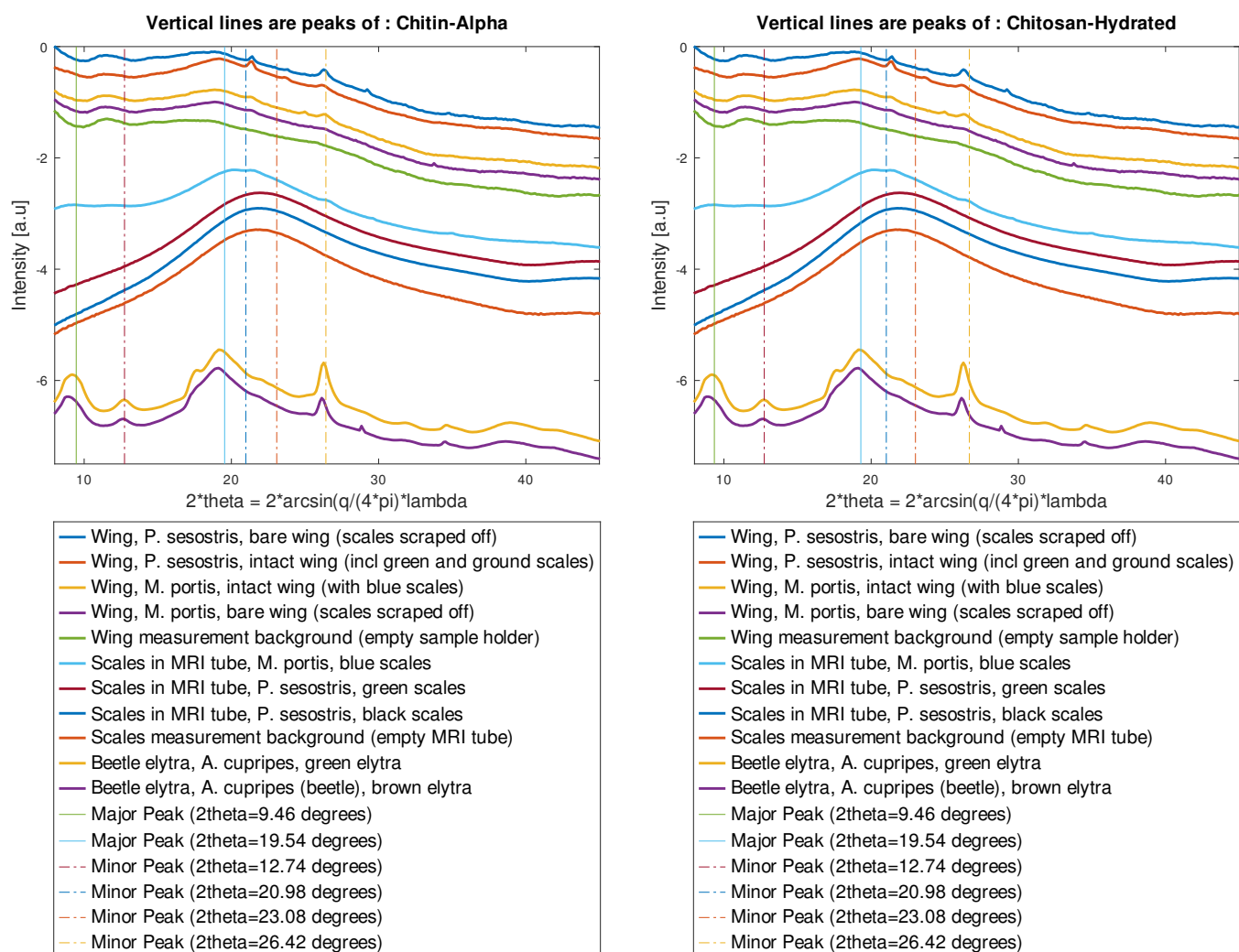


Fig. S6. Azimuthally averaged X-ray scattering intensity of sections of butterfly wings (with and without scales removed), of a powder sample of intact butterfly wing scales in an MRI tube and, as a reference, of sections of the elytra of *Anomala cupripes* (green cuticle and brown cuticle). All were obtained from dried specimens of the adult animals that had undergone normal development. The *Parides sesostris* scales were collected from circa 30 specimens and were a mixture of butterflies collected in Panama as part of this project, and specimens purchased from World of Butterflies (wobam.co.uk) labelled as originating from Peru, and of *Morpho portis* specimens. Specimens of *M. portis* were samples previously purchased from an unknown commercial insect supplier. The beetle specimens of *A. cupripes* were added as a reference for a biological material with a Bouligand reflector structure. Intensities are in arbitrary units on a logarithmic scale, with curves shifted up or down to enable better visibility. Data was compared to all chitin and chitosan phases described in Table 1 of (2). The two plots are the same scattering data, and differ only in the vertical line that indicate the major and minor peaks of 'alpha chitin' (left) and 'chitosan hydrated' (right). Among the phases discussed in (2) only these two provide reasonably similar peak positions to the peaks of the beetle data. The powder samples of scales of *P. sesostris* show no indication of any crystalline order. The powder sample of scales of *M. portis* shows some tiny peaks that may relate to an underlying small crystalline contribution of the constituent material, but are not clearly related to a chitin phase. The wing samples for both butterfly species, both with and without scales, show some peaks which however do not clearly relate to a chitin phase. (For identification in black/white print: legends are in order of the vertical position of the scattering curves, with the bare wing sample of *P. sesostris* the top curve and the brown elytra of *A. cupripes* at the bottom.)

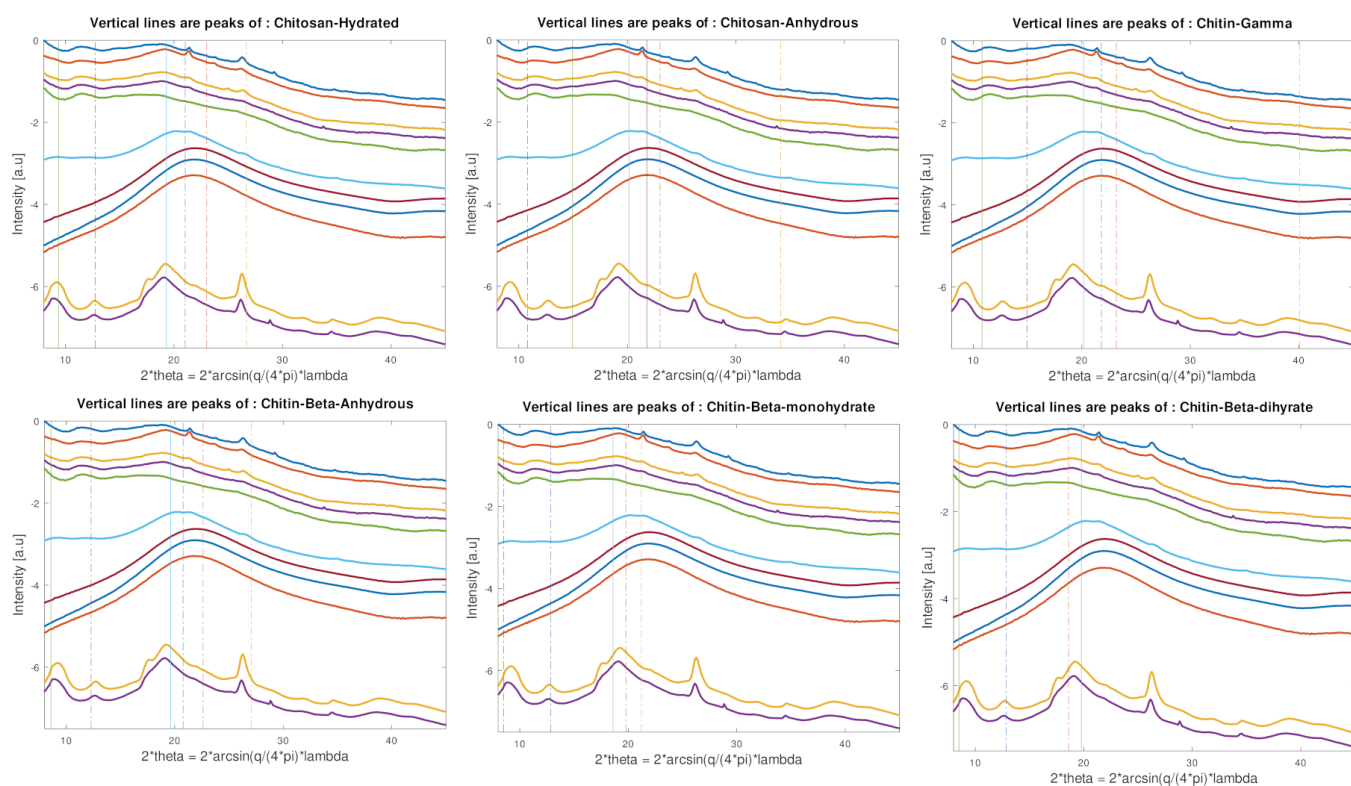


Fig. S7. The same X-ray scattering data as in Fig. S6, presented together with vertical lines representing other, less well fitting, phases as per (2). See Fig. S6 for legends.

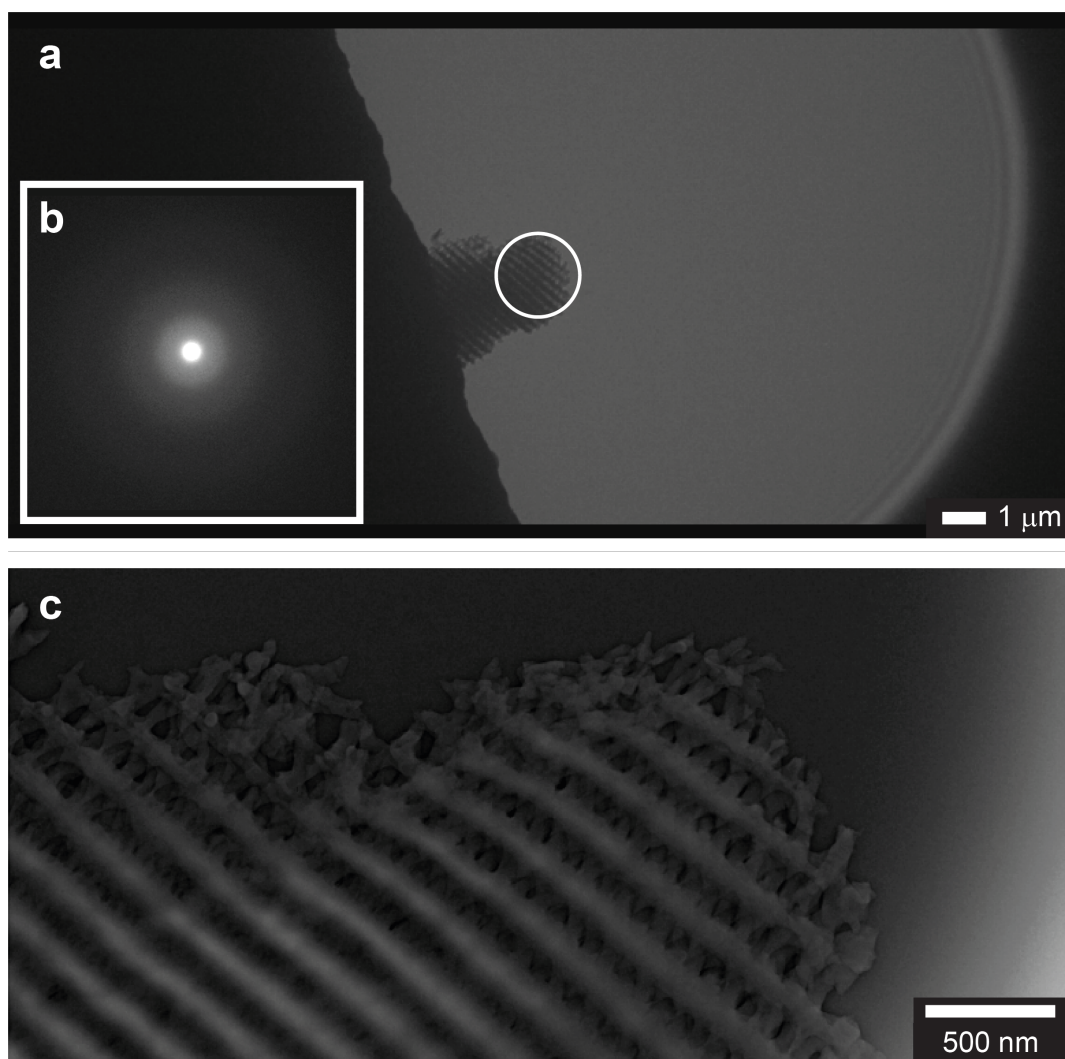
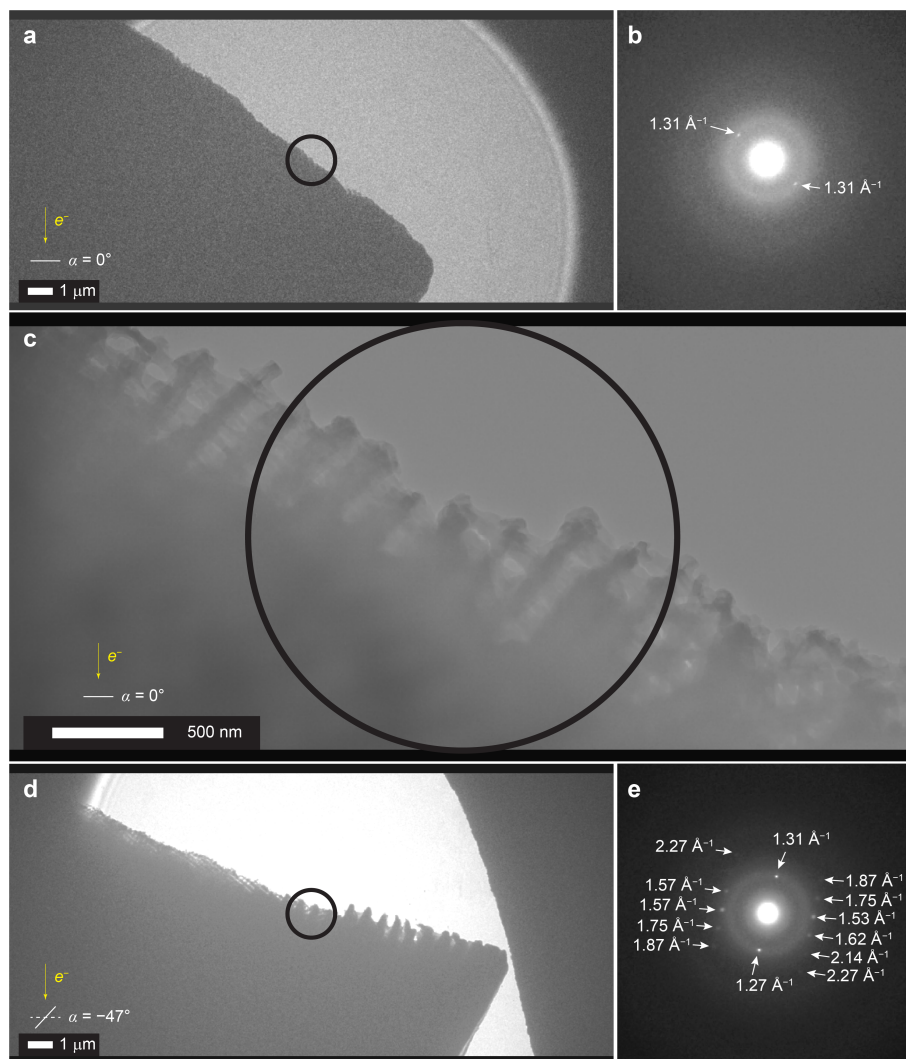


Fig. S8. Electron diffraction analysis carried out on gyroid-containing fragments in mature dry *P. sesostris* wing scales: a typical example of a gyroid fragment found in the dedicated electron diffractometer, after green scales from mature butterflies were gently ground between two glass slides. Two real-space images are presented (a and c) of the same fragment (at different magnifications), and the inset (b) shows the image acquired when the optics were switched to project diffracted waves onto the detector (showing only the primary beam and diffuse scattering). The white circle in panel (a) represents the area selected during the diffraction imaging (b).



	$2\theta_{\lambda=0.0251\text{ \AA}} / ^\circ$	$d / \text{\AA}$	$Q / \text{\AA}^{-1}$	$"2\theta_{\lambda=1.54\text{ \AA}}" / ^\circ$
a	0.30	4.79	1.31	18.5
a'	0.29	4.96	1.27	17.9
b	0.35	4.11	1.53	21.6
b'	0.36	3.99	1.57	22.2
c	0.37	3.89	1.62	22.9
c'	0.36	3.99	1.57	22.2
d	0.40	3.59	1.75	24.7
d'	0.40	3.59	1.75	24.7
e	0.43	3.34	1.87	26.6
e'	0.43	3.34	1.87	26.6
f	0.49	2.93	2.14	30.4
g	0.52	2.77	2.27	32.3
g'	0.52	2.77	2.27	32.3

The scattering vector $Q = (4 \pi / \lambda) \sin \theta$.

Fig. S9. Electron diffraction analysis carried out on gyroid-containing intact (but broken) scales in mature dry *P. sesostris* wing scales: images of one of the very few instances of gyroid-containing green scales from a mature *P. sesostris* wing which showed fleeting diffraction at $\alpha \approx 47^\circ$. Panels a and c show the scale at neutral tilt ($\alpha \approx 0^\circ$), with the diffraction image acquired at this angle shown in panel (b). Panel (d) shows a real-space image of the scale at $\alpha \approx 47^\circ$, where a number of Bragg peaks were observed in the diffraction image (e). In the real-space images (panels a, c and d), the area selected during the diffraction imaging is shown by black circles, and in the diffraction images (panels b and e) the scattering vectors, Q for weak Bragg peaks are annotated. The table below shows the 2θ angles for the reflections observed in panel (e), the equivalent d spacing (\AA) and scattering vectors ($Q / \text{\AA}^{-1}$), and the corresponding 2θ angles for $\lambda = 1.54 \text{\AA}$ (as used in the X-ray Scattering studies).

Step	Time	Watts	Load cooler	Vacuum
PBS rinse	40 sec	100	Yes	No
50% Ethanol	40 sec	150	Yes	No
70% Ethanol	40 sec	150	Yes	No
90% Ethanol	40 sec	150	Yes	No
100% Ethanol (anhydrous)	40 sec	150	Yes	No
100% Ethanol (anhydrous)	40 sec	150	Yes	No

Table S1. PELCO Biowave protocol for SEM sample preparation.

Step	Time	Watts	Load cooler	Vacuum
PBS rinse	40 sec	100	Yes	No
1% OsO ₄ in PBS	2 min on	100	Yes	Yes
1% OsO ₄ in PBS	2 min off	0	Yes	Yes
1% OsO ₄ in PBS	2 min on	100	Yes	Yes
1% OsO ₄ in PBS	2 min off	0	Yes	Yes
1% OsO ₄ in PBS	2 min on	100	Yes	Yes
Water rinse x 3	40 sec	100	Yes	No
70% Ethanol	40 sec	150	Yes	No
90% Ethanol	40 sec	150	Yes	No
100% Ethanol (anhydrous)	40 sec	150	Yes	No
100% Ethanol (anhydrous)	40 sec	150	Yes	No
100% Acetone (anhydrous)	40 sec	150	Yes	No
100% Acetone (anhydrous)	40 sec	150	Yes	No
Acetone: Resin 3 - 1	3 min	350	Yes	Yes
Acetone: Resin 1 - 3	3 min	350	Yes	Yes
Resin 100%	3 min	350	Yes	Yes

Table S2. PELCO Biowave protocol for TEM sample preparation.

18 Movie S1. Animation of a thin slice of the six-threaded $(0.8/6)^6$ weaving. The slice is in the $[110]$ direction
19 and is thinner than a unit cell size. The red and green arrows are the lattice translations $(-1,1,3)/2$ and
20 $(-1,1,-1)/2$, respectively, both within the $[110]$ plane.

21 Movie S2. Animation of a $2 \times 2 \times 2$ unit cell section of the six-threaded $(0.8/6)^6$ weaving on the srs net. The
22 movie shows the construction of the six-threaded weaving from individual helices winding around one of the
23 six $[110]$ axes.

24 SI Dataset S1 (SkeletalGraph_srsNet_latticeparameter1_FigureS3_ply.txt)

25 SI Dataset S2 (WovenStructure_0.8_over_6_FigS3AtoD_ply.txt)

26 SI Dataset S3 (WovenStructure_1.8_over_6_FigS3EtoF_ply.txt)

27 References

- 28 1. M Saba, BD Wilts, J Hielscher, GE Schröder-Turk, Absence of circular polarisation in reflections of butterfly wing scales
29 with chiral gyroid structure. *Mater. Today: Proc.* **1**, 193–208 (2014).
- 30 2. MV Tsurkan, et al., Progress in chitin analytics. *Carbohydr. Polym.* **252**, 117204 (2021).